Mon. Not. R. Astron. Soc. **331,** 569–577 (2002)

Quasar environment in the context of large-scale structure at $z \sim 0.3$

Ilona K. Söchting,[1★] Roger G. Clowes[1] and Luis E. Campusano[2]
[1]*Centre for Astrophysics, University of Central Lancashire, Preston PR1 2HE*
[2]*Observatorio Astronómico Cerro Calán, Departamento de Astronomía, Universidad de Chile, Casilla 36-D, Santiago, Chile*

Accepted 2001 November 5. Received 2001 November 2; in original form 2001 October 7

ABSTRACT

We look at quasar environment in the context of large-scale structure (LSS) – a new approach, giving a more informed interpretation of quasar–galaxy correlations. This paper presents our first results for a sample of $z \sim 0.3$ quasars. We use Voronoi tessellation applied in colour ($B_J - R$) slices for the detection of galaxy clusters and the minimal spanning tree (MST) to delineate the large-scale structure. This new cluster detection method allows us to find reliably galaxy clusters at $z < 0.3$ from SuperCOSMOS measurements of UK Schmidt Telescope plates. By reconstructing the large-scale structure in a relatively narrow redshift band ($0.2 < z < 0.3$), we show that quasars follow the large-scale structure traced by galaxy clusters. None of the quasars in our radio-quiet sample is located in the central area of a galaxy cluster. Two quasars, found in a very rich environment, are actually located between two very close galaxy clusters, consistent with results on $z \sim 1$ quasars, suggesting that cluster mergers may be involved in one of the quasar formation mechanisms.

Key words: methods: miscellaneous – galaxies: clusters: general – quasars: general – large-scale structure of Universe.

1 INTRODUCTION

Quasar environments have been studied on different scales, from those of the host galaxy to those of the quasar–cluster cross-correlation function. Yee & Green (1984) found that there is a difference in richness between the environments of radio-quiet and radio-loud quasars (RQQs and RLQs, respectively). This result has been confirmed by Ellingson, Yee & Green (1991), showing that RQQs are much less frequently situated in very rich galaxy clusters than RLQs. Confirmation came also from Hintzen, Romanishin & Valdes (1991), who found a significant excess of galaxies in the vicinity of RLQs, and from Boyle & Couch (1993), who found no significant excess of faint galaxies in association with RQQs. Hutchings, Crampton & Johnson (1995) obtained a different result; they observed the galaxy environment of RLQs and RQQs and concluded that there is no significant difference in the richness. Since the RQQs in that sample were members of a large quasar group (LQG) (Crampton, Cowley & Hartwick 1989, 1987), this result raised the question of whether the environments of members of LQGs could be different. However, some of the more recent results for quasars in general imply that the richness of the environments of radio-loud and radio-quiet quasars could indeed be very similar (e.g. Saxton, Hall & Turner 1999; Wold et al. 2001), whereas others still support the scenario of RLQs inhabiting more dense groups of galaxies than RQQs (Hutchings et al. 1999; Teplitz, McLean & Malkan 1999; Sánchez & Gomzáles-Serrano 1999).

The above results have been obtained using galaxy counts or the quasar–galaxy cross-correlation function within small radii ($< 1\,h^{-1}$ Mpc) around the quasars. The interpretation of the results is not a straightforward task, because of the erasure of directional information. For example, quasars residing centrally in poor clusters would produce similar statistics to those on the peripheries of very rich clusters.

Originally, the two-fold environment of quasars was interpreted as supporting the connection of RLQs with elliptical host galaxies and RQQs with spirals (e.g. Ellingson et al. 1991). However, in the past few years evidence has emerged that RQQs may have diverse host galaxies. In a sample studied by Bahcall et al. (1997), for example, more RQQs have been found in elliptical hosts than in spirals. The result has been confirmed by Boyce et al. (1998) and by McLure et al. (1999), who found that, just like radio-loud quasars, essentially all RQQs with luminosities greater than $M_R = -24$ reside in massive ellipticals. In many cases the host galaxies show traces of continuing interactions or past mergers (e.g. Bahcall et al. 1997; Boyce et al. 1998; Hutchings et al. 1999). Even if the host galaxies appear in the optical passbands to be isolated and apparently undisturbed, they are found to exhibit continuing or remnant tidal H I disruptions, indicating galactic encounters or mergers (Lim & Ho 1999).

The emerging picture is that RLQs have elliptical host galaxies and prefer a cluster environment, whereas the RQQs inhabit various host galaxies in a wide range of environments. At present

★E-mail: imachura@uclan.ac.uk

we have no information on how the close environment ($<1\,h^{-1}$ Mpc) of quasars is related to the large-scale structure traced by galaxy clusters, and if indeed the local enhancements of the density in the vicinity of quasars can be interpreted as galaxy clusters. This prompted us to introduce a new approach and look at the environments of quasars in the context of large-scale structure (LSS).

At low redshift, the LSS can be conveniently recognized as density peaks in multidimensional parameter space (RA, Dec., magnitude, colour) (Gladders & Yee 2000). Wide coverage (over $6\times6\,\mathrm{deg}^2$) is required to ensure the isotropic detection of structures on scales $\sim60\,h^{-1}$ Mpc. In this paper we describe our first results from this new approach. The quasar and galaxy samples used in this study are described in Section 2. The galaxy cluster detection method, including a short introduction to Voronoi tessellation, is outlined in Section 3. In Section 4 we have compiled the cluster catalogue from which the LSS has been reconstructed. The results of the study of the environments of quasars are contained in Sections 5 and 6. The advantages of the new approach and the implications of our results are discussed in Section 7. Throughout this paper we adopt a standard cosmological model with $\Omega=1$ and $H_0=100\,h\,\mathrm{km\,s^{-1}\,Mpc^{-1}}$.

2 DATA

Our quasar sample consists of 15 low-redshift ($z<0.4$) quasars from two surveys covering most of ESO/SERC field 927 (1950 field centre $10^{\mathrm{h}}40^{\mathrm{m}}00^{\mathrm{s}}$ $+05°00'00''$). Five quasars are from the AQD survey, which uses Automated Quasar Detection (AQD – Clowes 1986; see also Clowes, Cooke & Beard 1984). The spectroscopic observation of high-grade candidates was carried out at the CTIO 4-m telescope (Clowes & Campusano 1991, 1994; Clowes, Campusano & Graham 1999). Eight quasars come from the Chile–UK Quasar Survey (CUQS – Newman et al. 1998; Newman 1999), which uses the ultraviolet excess (UVX) method for selection. The spectroscopic observations were carried out at the Las Campanas 2.5-m Du Pont Telescope. Two quasars have come from Keable (1987). The CTIO quasars have faint limits ($B_{\mathrm{J}}\sim20.5$ mag) and sparse sampling, whereas the LCO quasars have bright limits ($B_{\mathrm{J}}\sim19.5$ mag) and complete sampling. The quasar sample will be incomplete, but, nevertheless, free of any spatial bias. Table 1 contains the basic information about the quasars in our sample.

Objects for the determination of the density distribution have been drawn from UK Schmidt Telescope (UKST) B_{J} and R plates covering $\sim6.3\times6.3\,\mathrm{deg}^2$ of sky. The plates have been digitized on the SuperCOSMOS measuring machine at the Royal Observatory Edinburgh. Only objects recognized on both plates became a part of the final catalogues. This process eliminates virtually all of the spurious detections in the individual plate scans (due to satellite and meteor trails, emulsion noise, etc.). The blue plates (J10128 and J10063) have been calibrated by applying third-degree polynomial fitting to deep (limiting $B_{\mathrm{J}}\sim21.5$ mag) charge-coupled device (CCD) sequences from Graham (1997). For the faint end ($B_{\mathrm{J}}>21.5$ mag) a linear extrapolation has been applied. The R plates (R18775 and R10071) have been calibrated in a similar way but using Keable (1987) data as secondary calibrators. The photometrically calibrated data set is limited at $B_{\mathrm{J}}=22.5$ mag and $R=21.5$ mag.

Star–galaxy separation is not reliable at such faint limits, but for the purpose of this study faint stars can be treated as forming a uniform background. Jones et al. (1991) found that the distribution of star counts in cells (small areas of size $4.96\times4.96\,\mathrm{arcmin}^2$), at similar galactic latitude to our study ($l\sim50°$), is close to that expected for a homogeneous Poisson distribution and that the variations of star counts are far lower than those of the galaxy counts. Considering that there are about three times as many galaxies as stars at the limiting magnitude ($B_{\mathrm{J}}=22.5$ mag), the assumption about the uniformity of the star distribution should be a good approximation.

3 FINDING GALAXY CLUSTERS

Galaxy clusters are the most massive gravitationally bound objects

Table 1. Low-redshift quasar sample. X and Y are the coordinates of the quasars in arcminutes from the field centre. The notation AQD/UVX means AQD quasars rediscovered by CUQS.

RA (J2000)	Dec. (J2000)	X (arcmin)	Y (arcmin)	z	B_{J} (mag)	Survey
10 33 56.8	+05 48 30	−130	64	0.376	19.3	AQD/UVX
10 34 47.9	+05 16 16	−117	32	0.331	19.2	AQD/UVX
10 34 58.3	+05 52 32	−114	68	0.297	19.5	UVX
10 35 06.0	+06 01 41	−112	77	0.245	18.9	UVX
10 36 15.7	+03 19 15	−95	−85	0.389	18.6	AQD
10 36 26.3	+04 54 35	−92	10	0.382	18.3	AQD
10 38 28.2	+04 45 35	−62	1	0.286	18.9	UVX
10 38 31.1	+06 09 12	−61	85	0.290	18.1	UVX
10 38 57.9	+04 48 39	−54	4	0.357	19.0	UVX
10 44 06.4	+03 14 50	23	−89	0.267		Keable
10 44 52.0	+03 52 51	34	−51	0.213	17.2	Keable
10 45 04.8	+04 34 01	37	−10	0.395	19.5	UVX
10 45 35.1	+03 41 22	45	−63	0.355	19.3	UVX
10 46 10.6	+03 50 31	54	−54	0.363	19.2	UVX
10 50 42.8	+04 17 39	122	−27	0.230	19.4	AQD/UVX

known, and are the obvious tracers of the LSS. They appear as peaks in the number density distribution of galaxies. Since we are interested in the position of quasars with respect to cores of galaxy clusters and want to resolve the subclusters if present, it is crucial to preserve the topological information when sampling the density distribution. The Voronoi tessellation has been chosen, since it is a non-parametric method. Voronoi tessellation, also known in computational geometry as Dirichlet tessellation, provides a partition of a point pattern according to its spatial structure. Features of this kind of decomposition can also be used for analysis of the underlying point process and provide a non-parametric approach to complex point processes, such as galaxy clustering.

Given a set $\boldsymbol{S}$ of n distinct points in $\mathcal{R}^d$, the Voronoi diagram is the partition of $\mathcal{R}^d$ into n polyhedral regions $a(p)$ for ($p \in \boldsymbol{S}$). Each region of $a(p)$, called the Voronoi cell of p, is defined as the set of points in $\mathcal{R}^d$ that are closer to p than any other points in $\boldsymbol{S}$:

$$a(p) = \{x \in \mathcal{R}^d \mid \bar{r}(x,p) \leq \bar{r}(x,q) \ \forall \ q \in \boldsymbol{S} - p\}$$

where $\bar{r}$ is the Euclidean distance function (Okabe et al. 2000, and references therein). One can use different distance functions to define various variations of Voronoi diagrams, but they will not be discussed here. The set of all Voronoi cells and their faces forms a cell complex. The vertices of this complex are called the Voronoi vertices, and the extreme rays (i.e. unbounded edges) are the Voronoi edges.

A useful application of the Voronoi model is the compilation of surface density maps from point data. If one generates the Voronoi diagram of the point set $\boldsymbol{S}$ and measures the area A_i of each polygon a_i, one can consider A_i^{-1} as an indicator of the local intensity of the point pattern at a_i (Duyckaerts, Godefroy & Hauw 1994). Using the astrophysical nomenclature, A_i is the local number density at the position of the object i from the sample.

The Voronoi tessellation diagrams permit the generation of contour plots of the density distribution without gridding the data. Gridding of data introduces, in many cases, undesired smoothing and parametrization, which distort the morphology of the measured distribution.

The Voronoi tessellation has been used successfully for finding galaxy clusters (Kim et al. 2000; Ramella et al. 2001) and its performance compared with that of the matched filter method by Ramella et al. (2001). In contrast to Ramella et al. (2001), we detect galaxy clusters by thresholding of the density contours in colour slices and not in magnitude slices. The use of colour slices has been proposed and tested by Gladders & Yee (2000). Selecting galaxies in colour slices in the colour–magnitude diagram increases the density contrast of any grouping of early-type galaxies, which are normally found in clusters or groups. A colour slice in the colour–magnitude plane provides separation in redshift space via the red sequence of early-type galaxies in clusters (Gladders & Yee 2000, and references therein), thus reducing considerably the projection effects.

The redshift range $0 < z < 0.4$ corresponds to a $B_J - R$ colour space in the range $1.4\,\mathrm{mag} < B_J - R < 2.5\,\mathrm{mag}$ using the galaxy colours derived by Fukugita, Shimasaku & Ichikawa (1995). The limit in the redshift space for this pair of filters is $z \sim 0.4$, since the colours for higher-redshift ellipticals start to drop for $z > 0.6$, reaching $B_J - R \sim 2.5\,\mathrm{mag}$ again at $z \sim 0.8$. Such high-redshift clusters are in any case beyond the magnitude limit of our data. Using the colours of the known clusters and the model predictions (Kodama et al. 1998), the appropriate gradient of the slices in the colour–magnitude plane has been deduced to be -0.06. The width of the slices is mainly dictated by the uncertainties in the photometric calibration and empirically selected to be $\Delta(B_J - R) = 0.2\,\mathrm{mag}$. The colour slices are overlapping in steps of 0.1 mag.

The analysis is performed initially in every colour slice separately. The points belonging to candidates for galaxy clusters are selected as those exceeding an intensity threshold $(2/n)\sum_{i=1}^{n} a_i^{-1}$, where a_i is the area of the ith polygon (corresponding to the ith object) and n is the total number of points (polygons). This threshold corresponds to $(N_{\mathrm{field}} + N_{\mathrm{cluster}})/N_{\mathrm{field}} \sim 2$, where N_{field} is the number density of field galaxies integrated in the line of sight to $z = 0.3$ and N_{cluster} is the number density of the core of a poor cluster. The literature values for the densities have been adopted from Cox (1999). Fig. 1 illustrates the distribution of the densities in a typical colour slice and the selected threshold, which usually picks ~ 5 per cent of the cells in the slice.

The colour–magnitude relation applies to the elliptical galaxies, which in turn are known to form the cores of the clusters. The cluster cores can be expected to be mathematically closed (no holes or single-object dips in the boundary) structures. Strongly non-virialized clusters, such as Virgo, consisting of multiple subclusters, may be considered as associations of multiple separated cores. The algorithm employed to close the boundaries of the cores is based on the principle that detected structures are closed if all cells with a simple majority of its natural neighbours (adjacent cells) exceeding the density threshold are being included in the selection.

The Voronoi tessellation has the power to detect groupings on the richness scale from loose groups to rich clusters. To find only groupings that qualify as clusters, a lower limit on the number of interconnected objects in a cluster must be introduced. The lower limit for a poor cluster (Abell class 0) is by definition 30 galaxies. To detect such poor clusters with an ellipticals content as low as 25 per cent, a minimum of seven interconnected objects is required. The results from all the colour slices have been combined according to the principle that two clusters from different slices sharing two or more members constitute the same cluster.

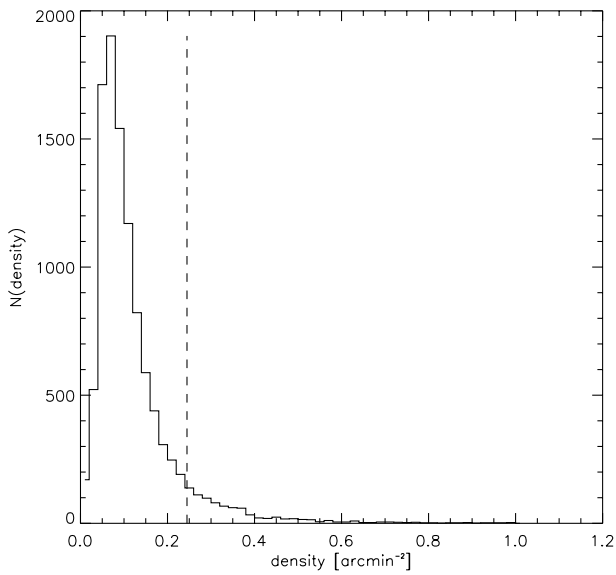

Figure 1. Histogram illustrating the distribution of the Voronoi densities in a typical colour slice ($1.9 < (B_J - R)/\mathrm{mag} \leq 2.1$ in this example). The dashed vertical line indicates the threshold density.

4 CLUSTER SAMPLE

The application of the above procedure to the $\sim 36\,\mathrm{deg}^2$ area of investigation produced a sample of 72 galaxy clusters with estimated redshifts in the range $0.03 \leq z \leq 0.37$. The resulting density is 2.0 cluster deg^{-2} with $\langle z \rangle = 0.19$. Because of the magnitude limit, only 13 (optically brightest) clusters with $z > 0.3$ have been detected. Fig. 2 shows some examples of the detected clusters with different morphologies and redshifts.

The data for all the detected clusters have been compiled in Table 2. The positions are expressed in RA and Dec. (J2000) and as *X* and *Y*, which are the coordinates in arcminutes from the field centre (used in all figures). The area of a cluster core is here defined as the area of the convex hull enclosing all the Voronoi cells of the early-type galaxies found to be members of the cluster. It gives a good measure of the core of the cluster, preserving its morphology. The number of galaxies (N_G) in a cluster core is here defined as the background-corrected number of objects found within the convex hull defining the boundary of the core. The radius (R_P) is the minimum radius necessary to enclose the whole convex hull. The colours of the red sequences have been established by inspection of the colour–magnitude plots for every cluster. The redshift z has been estimated using the red sequence approach and the colours of elliptical galaxies compiled by Fukugita et al. (1995). The uncertainty of the estimate is ~ 0.05 as a result of the uncertainties in the photometric calibration. The Abell richness (N_R) of the clusters has been computed using the estimated redshifts to calcucate the angular extent of the Abell radius ($1.5\,h^{-1}\,\mathrm{Mpc}$). The background counts, used for background corrections, have been taken as those of a region without any detected clusters. The identifications of the previously known clusters have been indicated in the final column.

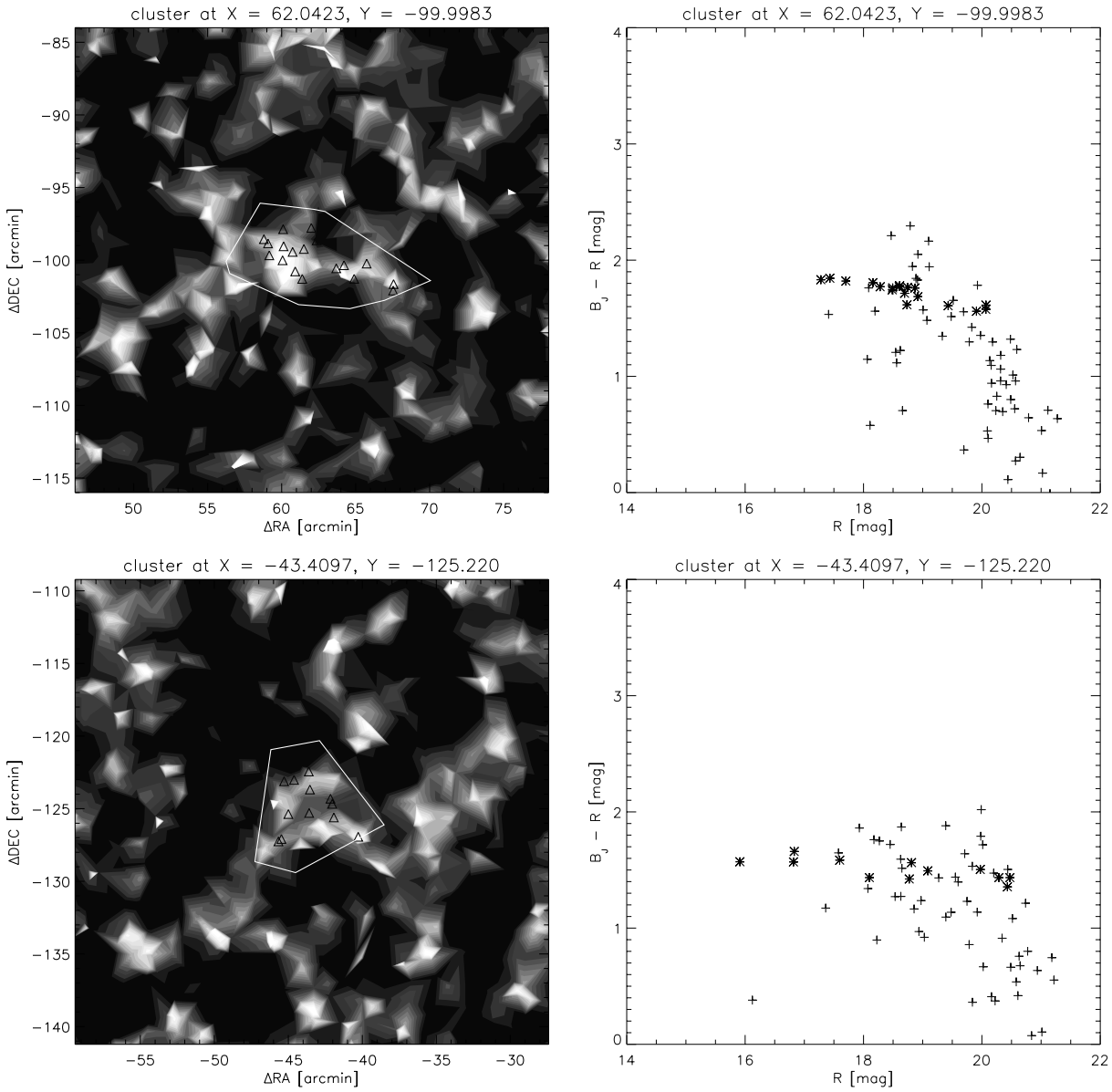

Figure 2. Two examples of detected clusters. For each cluster, the panel on the left is a contour plot of the density distribution, with the polygon enclosing the core of the cluster with early-type galaxies (triangles). The panel on the right is a colour–magnitude diagram of all objects contained in the polygon, with those objects indicated by asterisks defining the cluster detection.

The area of investigation contains 16 published galaxy clusters, three of which have known redshifts. We identified 14 of these clusters, including all those with known redshifts. The two clusters we could not identify may be spurious since they were detected only as density peaks in two dimensions or have few ellipticals and so are below our threshold in the colour slices. Fig. 3 gives the comparison of the published centres of the clusters and those determined using colour slices. The difference is strongest for the lowest redshift cluster ($X = 81$, $Y = 22$, $z = 0.03$); most of the other clusters agree very well. The three known redshifts (0.03, 0.07, 0.15) allowed an improvement of our redshift estimate at $z < 0.2$ by direct calibration of the colour–redshift sequence.

5 THE LARGE-SCALE ENVIRONMENT OF QUASARS

The purpose of our investigation is to establish whether quasars trace the same structures as the galaxy clusters. The quasar sample covers the redshift range $0.2 < z < 0.4$. However, the cluster sample appears to be very incomplete at $z > 0.3$, forcing us to limit the main investigation to one redshift slice, $0.2 < z < 0.3$. The area of the quasar survey is smaller than that populated by detected clusters. Only objects in the common area ($\sim 25\,\mathrm{deg}^2$) of both quasar and cluster samples have been selected for the environmental study. The final sample comprises 17 galaxy clusters and seven quasars (Fig. 4).

The problem of connecting discrete objects into a continuous structure can be approached using another graph theoretical method, the minimal spanning tree (MST). This method has been successfully tested for finding LQGs in quasar samples (Graham 1997). The MST is a geometric construct, originating in graph theory, which was introduced by Kruskal (1956) and Prim (1957).

In our case the nodes of the MST are the galaxy clusters. For the purpose of this study we did not attempt to separate the MST to recover the galaxy superclusters, but preserved the continuous LSS. When looking at Fig. 4, it can be seen that quasars populate the region delineated by the MST as LSS. In order to test the statistical significance of this result, we resampled the quasar distribution using a Monte Carlo method. As a measure of how close the quasars follow the LSS, we have used the sum of the distances between quasars and their closest MST edges $\sum_{i=1}^{n} r_i$. The result of 100 000 simulations has been plotted as a histogram in Fig. 5. The test rejects the null hypothesis that the quasars are distributed independently of the LSS in clusters at a level of significance of 0.009.

6 SMALL-SCALE ENVIRONMENT OF QUASARS

From Fig. 4, it can be seen that the quasars appear to avoid the central density peaks of the clusters, and reside instead in two types of environments. Most of them (five out of seven) reside on the distant (3–$5\,h^{-1}$ Mpc) peripheries of the galaxy clusters tracing the same LSS. This is an important result, suggesting that the topology of the density field in the quasar environments might be a crucial parameter connected with the triggering of quasar formation and the controlling of their evolution. Some of the quasars (two out of seven), however, are found between two very close clusters. Such an arrangement suggests that quasar formation might also be associated with cluster mergers.

Fig. 6 illustrates the density distribution and the two close clusters around a quasar at $z = 0.245$. The estimated redshifts of both galaxy clusters are comparable to that of the quasar, suggesting that all three objects are physically associated.

The second merger candidates are more difficult to verify. Both clusters found in the vicinity of a quasar at $z = 0.286$ (Fig. 7) are obscured by foreground clusters. They have clear red sequences in the colour–magnitude diagram but the enclosing polygons and redshift estimates are nevertheless less reliable than in the first case outlined above. The redshifts of both clusters are estimated to lie in the range $0.25 < z < 0.30$, which is compatible with the redshift of the quasar.

This result suggests that quasars found in rich environments are actually not in the centres of galaxy clusters but mark the regions of cluster/subcluster mergers by residing between two (or more) density peaks. With only two quasars, however, this needs to be confirmed with a larger sample (work in progress).

7 DISCUSSION AND CONCLUSIONS

The majority of the studies of the richness of the environments of quasars have relied on counting galaxies within a quite small radius ~ 1 Mpc without consideration of the morphology of the distribution. Such an approach provides a fast means of tabulating and comparing the richness within large data sets. However, to ensure a correct interpretation of the results, we must determine what physical structures in the galaxy distribution are associated with quasars. We have studied the association of quasars with optically detected clusters of galaxies. By reconstructing the LSS in a relatively narrow redshift band ($0.2 < z < 0.3$), we have been able to show that quasars follow the large-scale structure traced by galaxy clusters. The quasar–cluster LSS investigated in this paper is on the scale of superclusters ($\sim 60\,h^{-1}$ Mpc), which suggests that quasars could be used to trace the distribution of superclusters. Oort, Arp & de Ruiter (1981) put forward for the first time the hypothesis that quasars are located in superclusters using the statistics of close quasar pairs as evidence. It is normally expected that clusters of galaxies trace mass, and that the LSS of galaxies also traces mass. Our results show that quasars trace the mass (galaxies) on supercluster scales for low redshifts $z \lesssim 0.3$. It means that the formation/fuelling process of quasars is coupled, at low redshift, to the large density perturbations, which makes quasars useful indicators of mass at $z \lesssim 0.3$. We should not, however, simply extend this conclusion to higher redshifts without observational support because the relative importance of different mechanisms for quasar formation will almost certainly vary with redshift.

Secondly, none of the quasars in our radio-quiet sample is located in the central area of a galaxy cluster. Apart from the two quasars found between merging clusters, all the others reside on the distant (3–$5\,h^{-1}$ Mpc) peripheries of galaxy clusters. The peripheral position of RQQs in relation to galaxy clusters was first noticed by Yee & Green (1984) when assessing by eye the distribution of companion galaxies in the vicinity of quasars. Yee (1992) noticed that $z \sim 0.6$ quasars do not reside close to the cD galaxies marking the centres of clusters, but these results do not seem to have been pursued further. Hashimoto & Oemler (2000) found that galaxy interactions are more likely in galaxy groups and very poor clusters. They found also about the same ratio of interactions in rich clusters as in the field, three times less than in groups and poor clusters. The fact that most quasars in our sample (five out of seven) strongly avoid the rich environments of the central regions of galaxy clusters is compatible with models connecting the majority of low-z quasars with galaxy groups and suggesting that

Table 2. Cluster sample.

RA (hh mm)	Dec. (dd mm)	X (arcmin)	Y (arcmin)	Area (arcmin^2)	N_G	R_P (arcmin)	z	N_R	ID Zwicky
10 31.3	+05 16	−168	32	21	31	1.9	0.22	34	–
10 31.5	+03 46	−165	−58	40	46	3.3	0.07	97	–
10 32.1	+04 26	−156	−18	37	44	2.8	0.22	22	–
10 32.4	+04 59	−151	16	43	75	2.8	0.20	21	3280
10 32.5	+02 42	−149	−122	25	29	2.2	0.12	11	–
10 32.8	+02 36	−146	−128	26	40	2.4	0.12	60	–
10 33.0	+02 12	−143	−152	56	99	3.1	0.15	44	–
10 33.0	+05 59	−142	75	61	67	3.8	0.17	33	–
10 33.3	+05 12	−139	28	30	45	2.9	0.17	19	–
10 33.4	+05 01	−137	17	27	43	2.7	0.20	34	–
10 33.9	+04 23	−129	−21	35	51	3.4	0.12	80	–
10 34.1	+05 39	−126	55	13	26	2.1	0.17	35	3290
10 34.7	+04 26	−117	−18	39	77	3.5	0.17	47	3287
10 34.7	+06 11	−116	87	23	57	1.7	0.22	25	3304
10 35.0	+04 39	−113	−4	43	50	3.1	0.07	191	–
10 35.1	+03 34	−111	−70	28	45	2.4	0.07	110	3303
10 35.3	+04 03	−108	−41	37	44	2.9	0.15	24	–
10 35.3	+03 55	−108	−49	30	23	2.8	0.17	40	–
10 35.4	+05 59	−106	75	32	39	2.4	0.20	26	–
10 35.5	+05 18	−105	34	87	87	4.7	0.32	24	–
10 36.2	+02 50	−95	−114	30	49	2.4	0.15	24	–
10 36.3	+03 11	−93	−93	38	77	2.7	0.22	10	–
10 36.3	+07 21	−93	157	39	52	2.6	0.15	28	–
10 36.6	+06 22	−88	98	25	32	2.1	0.20	27	–
10 36.7	+07 13	−87	149	26	47	2.6	0.15	40	3322
10 37.5	+05 46	−75	62	11	10	4.7	0.32	11	–
10 37.6	+04 07	−73	−37	31	42	2.8	0.22	48	–
10 38.3	+04 53	−63	9	44	45	2.5	0.07	235	–
10 38.3	+04 53	−63	9	24	30	2.5	0.27	235	–
10 38.5	+04 59	−60	15	24	36	2.7	0.07	245	–
10 38.6	+05 09	−58	25	30	32	2.1	0.22	52	–
10 38.9	+04 41	−54	−3	45	79	7.2	0.12	34	–
10 38.9	+04 41	−54	−3	25	39	3.2	0.27	24	–
10 39.1	+04 12	−52	−32	87	10	4.5	0.17	21	–
10 39.1	+02 19	−51	−145	39	55	2.9	0.12	48	3365
10 39.1	+05 13	−51	29	10	18	5.7	0.07	111	3367
10 39.6	+02 39	−43	−125	49	68	4.3	0.15	17	–
10 39.7	+03 47	−42	−57	24	28	2.2	0.17	76	–
10 39.9	+04 03	−39	−41	58	62	3.5	0.32	23	–
10 40.1	+03 42	−36	−62	13	14	5.9	0.32	13	–
10 40.5	+03 19	−30	−85	24	47	2.4	0.17	22	–
10 40.6	+04 24	−28	−20	67	83	4.3	0.32	23	–
10 40.7	+06 50	−27	126	56	59	3.8	0.37	14	–
10 40.9	+04 58	−25	14	28	38	2.1	0.32	6	–
10 41.8	+02 35	−10	−129	30	29	2.4	0.07	89	–
10 42.2	+07 24	−4	160	30	36	2.6	0.27	31	–
10 43.2	+03 40	12	−64	29	34	2.6	0.15	19	–
10 43.8	+04 12	19	−32	45	65	3.7	0.07	63	–
10 44.0	+04 35	21	−9	23	26	2.5	0.17	36	–
10 44.0	+07 05	23	141	52	63	3.8	0.32	21	–
10 44.5	+05 25	30	41	81	77	4.9	0.32	22	–
10 44.5	+05 44	30	60	46	53	3.3	0.32	16	–
10 44.5	+06 05	30	81	35	51	2.5	0.32	27	–
10 45.6	+04 18	46	−26	19	42	1.8	0.20	45	3448
10 46.0	+06 40	52	116	63	62	5.8	0.07	14	–
10 46.6	+03 04	62	−100	61	78	3.2	0.20	38	3460
10 47.9	+05 05	81	22	26	41	2.4	0.03	367	3477
10 48.0	+04 40	83	−4	52	78	3.7	0.07	165	–
10 48.4	+06 16	88	92	51	42	3.5	0.12	14	–
10 48.9	+07 13	96	149	43	67	3.0	0.22	38	3489

Table 2 – *continued*

RA (hh mm)	Dec. (dd mm)	X (arcmin)	Y (arcmin)	Area (arcmin^2)	N_G	R_P (arcmin)	z	N_R	ID Zwicky
10 49.0	+05 50	97	66	23	32	2.1	0.22	21	–
10 48.9	+07 23	97	159	33	54	2.9	0.20	21	–
10 49.3	+05 10	101	26	24	40	1.9	0.22	47	–
10 49.4	+03 40	103	−64	22	43	2.0	0.15	48	3502
10 49.5	+05 54	105	70	49	66	3.9	0.22	26	–
10 50.0	+05 25	112	41	29	47	2.1	0.22	50	–
10 50.1	+03 38	114	−66	23	31	2.2	0.07	183	–
10 50.5	+04 44	120	0	49	62	3.7	0.17	21	–
10 51.3	+05 06	132	22	34	76	3.1	0.37	21	3537
10 51.3	+03 41	132	−63	23	29	2.3	0.07	238	–
10 51.7	+05 18	138	34	46	61	2.9	0.32	22	–
10 51.9	+04 58	142	14	55	69	2.9	0.20	40	–

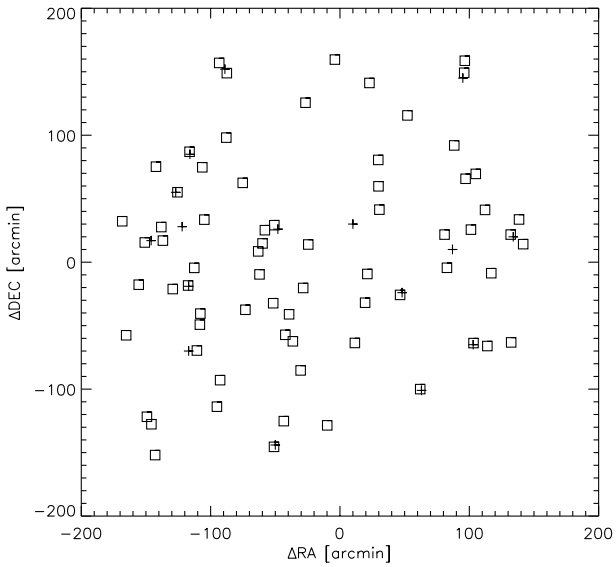

Figure 3. Cluster sample. The squares are centred on the galaxy clusters detected by Voronoi tessellation in $(B_J - R)$ colour slices. The overplotted plus signs represent the known galaxy clusters drawn from the CEDAG Catalogue of Clusters of Galaxies.

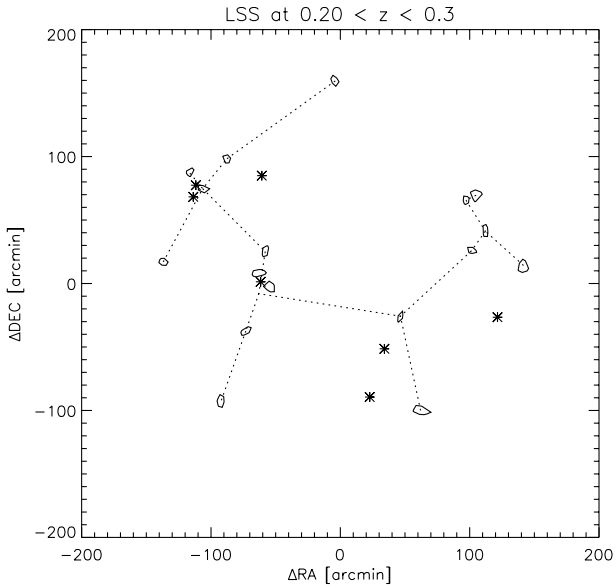

Figure 4. The relation between the LSS in galaxy clusters (polygons) delineated by the MST (dotted line) and quasars (asterisks) in the redshift slice $0.2 < z < 0.3$. The axes correspond to X and Y in units of arcminutes from the centre of ESO/SERC field 927.

major galaxy–galaxy mergers are the main, but not the only, mechanism of quasar formation at low z.

Lastly, we find that quasars found in very rich environments (two out of seven) may actually be located between two very close galaxy clusters. Owing to the relatively small number of quasars in our sample, it is not possible to draw conclusions about the percentage of such objects in the overall quasar population. Two clusters separated by a distance $< 2\,h^{-1}$ Mpc are expected to have entered already the pre-merger stage (Schindler 2001) in which strong gas compression accompanied by heating occurs. The high velocities of galaxies found in merging clusters do not favour major galaxy–galaxy mergers as a quasar formation mechanism, but rather point towards galaxy harassment (Lake, Katz & Moore 1998). However, cluster/subcluster mergers produce compression of hot gas between two subclusters shortly before they collide and shock waves after the collision (Schindler 1999). Considering the complex nature and the high energetics of the gas compressions and displacements already during the pre-merger stage of two galaxy clusters, we should consider also a model in which a quasar is formed in a galaxy–gas interaction. It has been argued that strong star formation can be triggered by the influence of dense intracluster medium (ICM) at the confluence of a cluster/subcluster merger (Evrard 1991). Our result for $z \sim 0.3$ quasars, combined with the fact that Haines et al. (2001) and Tanaka et al. (2000) found quasars on the peripheries of clusters at $z \sim 1.3$ and 1.1, with some being accompanied by a band of star-forming galaxies and some evidence again for cluster mergers, suggests that such a process could indeed be one of the quasar formation mechanisms.

To determine the relative contributions of the cluster-merger like and distant periphery like environments to the formation of quasars, we are planning to study a large quasar sample, spanning a wide redshift range. The inclusion of radio-loud quasars will allow us to quantify the results as functions of redshift and radio-loudness. Multiwavelength observations will be required to establish the role of the ICM in triggering the formation of quasars. The X-ray morphology of the merging clusters will give us

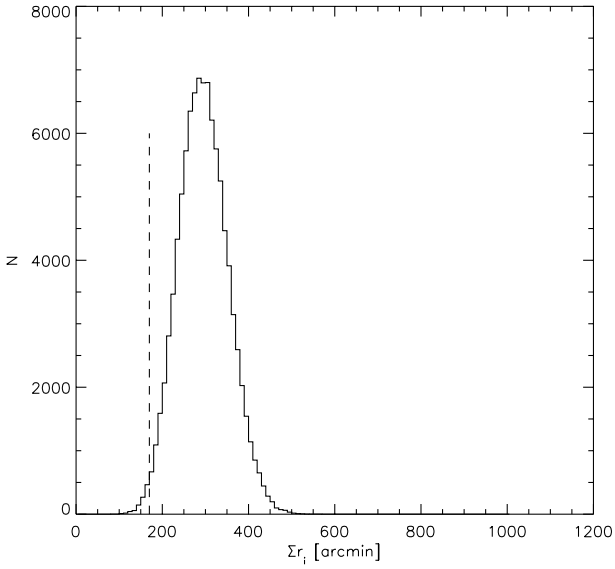

Figure 5. The result of the Monte Carlo resampling of the quasar distribution in relation to the MST vectors. The histogram illustrates the distribution of $\sum_{i=1}^{n} r_i$, where r_i is the distance of the ith quasar to its closest MST edge, in 100 000 simulation runs. The vertical dashed line indicates the value produced by the quasars in the real sample.

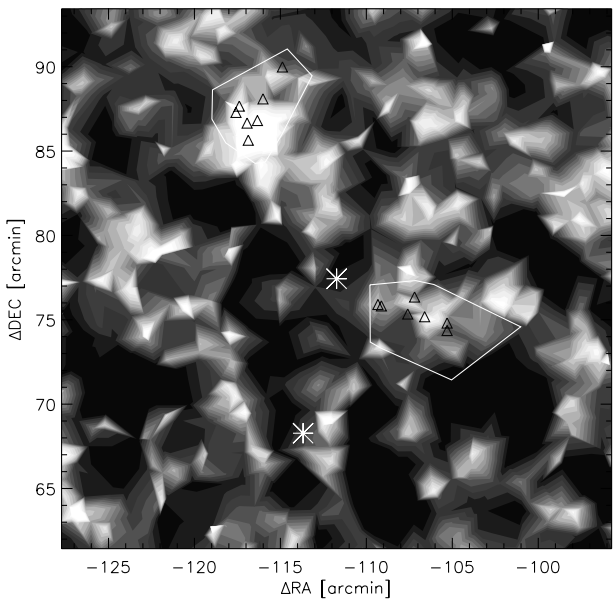

Figure 6. The environment of the quasar at $z = 0.245$. The figure shows the density distribution (filled contours) and the cores of two clusters (polygons) identified at a comparable redshift.

information about the distribution of the hot gas. Imaging of the host galaxies and their close companions will be used to find traces of recent mergers or interactions.

ACKNOWLEDGMENTS

IKS is funded by a bursary of the University of Central Lancashire, UK. LEC was funded partly by grant 1970/735 from the Fondo Nacional de Desarrollo Científico y Tecnológico, Chile. We would like to thank Francisco Castander for constructive discussion about the cluster detection method.

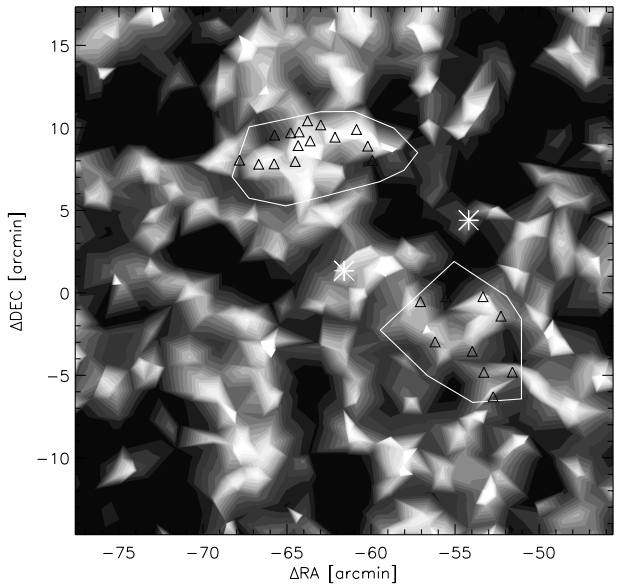

Figure 7. The environment of the quasar at $z = 0.286$. The figure shows the density distribution (filled contours) and the cores of two clusters (polygons) identified at a comparable redshift. The density enhancement superimposed on the position of the quasar is due to projection and does not form a cluster core.

REFERENCES

Bahcall J. N., Kirhakos S., Saxe D. H., Schneider D. P., 1997, ApJ, 479, 642
Boyce P. J. et al., 1998, MNRAS, 298, 121
Boyle B. J., Couch W. J., 1993, MNRAS, 264, 604
Clowes R. G., 1986, Mitt. Astron. Ges., 67, 174
Clowes R. G., Campusano L. E., 1991, MNRAS, 249, 218
Clowes R. G., Campusano L. E., 1994, MNRAS, 266, 317
Clowes R. G., Cooke J. A., Beard S. M., 1984, MNRAS, 207, 99
Clowes R. G., Campusano L. E., Graham M. J., 1999, MNRAS, 309, 48
Cox A. N., ed., 1999, Allen's Astrophysical Quantities, 4th edn. AIP Press, New York, Springer, Berlin
Crampton D., Cowley A. P., Hartwick F. D. A., 1987, ApJ, 314, 129
Crampton D., Cowley A. P., Hartwick F. D. A., 1989, ApJ, 345, 59
Duyckaerts C., Godefroy G., Hauw J.-J., 1994, J. Neurosci. Methods, 51, 47
Ellingson E., Yee H. K. C., Green R. F., 1991, ApJ, 371, 49
Evrard A. E., 1991, MNRAS, 248, L8
Fukugita M., Shimasaku K., Ichikawa T., 1995, PASP, 107, 945
Gladders M., Yee H. K. C., 2000, AJ, 120, 2148
Graham M. J., 1997, PhD thesis, Univ. Central Lancashire
Haines C. P., Clowes R. G., Campusano L. E., Adamson A. J., 2001, MNRAS, 323, 688
Hashimoto Y., Oemler A., 2000, ApJ, 530, 652
Hintzen P., Romanishin W., Valdes F., 1991, ApJ, 366, 7
Hutchings J. B., Crampton D., Johnson A., 1995, AJ, 109, 73
Hutchings J. B., Crampton D., Morris S. L., Durand D., Steinbring E., 1999, ApJ, 117, 1109
Jones L. R., Fong R., Shanks T., Ellis R. S., Peterson B. A., 1991, MNRAS, 249, 481
Keable C. J., 1987, PhD thesis, Univ. Edinburgh
Kim R. et al., 2000, in Mazure A., Le Fèvre O., Le Brun V., eds, ASP Conf. Ser. Vol. 200, Clustering at High Redshift. Astron. Soc. Pac., San Francisco, p. 422
Kodama T., Arimoto N., Barger A. J., Aragón-Salamanca A., 1998, A&A, 334, 99
Kruskal J. B., 1956, Proc. Am. Math. Soc., 7, 48
Lake G., Katz N., Moore B., 1998, ApJ, 495, 152
Lim J., Ho P. T. P., 1999, ApJ, 510, L7

McLure R. J., Kukula M. J., Dunlop J. S., Baum S. A., O'Dea C. P., Hughes D. H., 1999, MNRAS, 308, 377
Newman P. R., 1999, PhD thesis, Univ. Central Lancashire
Newman P. R., Clowes R. G., Campusano L. E., Graham M. J., 1998, in Colombi S., Mellier Y., Raban B., eds, 14th IAP Colloq., Wide Field Surveys in Cosmology. Editions Frontières, Gif-sur-Yvette, p. 408
Okabe A., Boots B., Sugihara K., Chiu N., 2000, Spatial Tessellations, 2nd edn. Wiley, Chichester
Oort J. H., Arp H., de Ruiter H., 1981, A&A, 95, 7
Prim R. C., 1957, Bell Syst. Tech. J., 36, 1389
Ramella M., Boschin W., Fadda D., Nonino M., 2001, A&A, 308, 776
Sánchez S. F., Gomzáles-Serrano J. L., 1999, A&A, 352, 383
Saxton R. D., Hall P. B., Turner M. J. L., 1999, in Giuricin G., Mezzetti M., Salucci P., eds, ASP Conf. Ser. Vol. 176, Observational Cosmology: The Development of Galaxy Systems. Astron. Soc. Pac., San Francisco, p. 389
Schindler S., 1999, in Giovanelli F., Sabau-Graziati L., eds, Proc. Volcano Workshop 1999, Multifrequency Behaviour of High Energy Cosmic Sources. In press (astro-ph/9909042)
Schindler S., 2001, in Neumann D. M., ed., Proc. XXI Moriond Conf., Galaxy Clusters and the High Redshift Universe. In press (astro-ph/0107008)
Tanaka I. et al., 2000, ApJ, 528, 123
Teplitz H. I., McLean I. S., Malkan M. N., 1999, ApJ, 520, 469
Wold M., Lacy M., Lilje P. B., Serjeant S., 2001, MNRAS, 323, 231
Yee H. K. C., 1992, in Fabian A. C., ed., Clusters and Superclusters of Galaxies. Kluwer, Dordrecht, p. 293
Yee H. K. C., Green R. F., 1984, ApJ, 280, 79

This paper has been typeset from a TEX/LATEX file prepared by the author.